Fuel 331 (2023) 125641

Contents lists available at ScienceDirect

Fuel

journal homepage: www.elsevier.com/locate/fuel

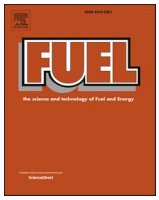

Full Length Article

Fuel property impacts on gaseous and PM emissions from a multi-mode single-cylinder engine

Yensil Park [a], Melanie Moses-DeBusk [a,*], Tommy Powell [a], James Szybist [a], Zhanhong Xiang [b], Junqing Zhu [b], Charles S. McEnally [b], Lisa D. Pfefferle [b]

[a] Oak Ridge National Laboratory – National Transportation Research Center, Knoxville, TN 37932 USA
[b] Department of Chemical and Environmental Engineering, Yale University, New Haven, CT 06520 USA

ARTICLE INFO

Keywords:
Multi-mode
ACI
Emissions
Particular matter
EC/OC
HC speciation

ABSTRACT

The U.S. Department of Energy's Co-Optima initiative has focused on improving fuel economy and vehicle performance while reducing emissions through the simultaneous development of emerging sustainable fuels with beneficial properties and advanced combustion strategies. A major thrust has been the development of advanced compression ignition (*ACI*) combustion strategies of gasoline range fuels in combination with spark-ignited (SI) combustion in a single engine capable of multi-mode operation to achieve high power density with enhanced part load efficiency. The aim of this study was to further the understanding of how emissions from both *ACI* and SI strategies operating on the same fuels in the same engine are impacted by different fuel properties. This investigation focused on particulate matter (PM) and gaseous hydrocarbon emissions from 6 different fuels across 3 different combustion modes on the same single-cylinder engine designed for multi-mode operation: SI combustion, partial fuel stratification (PFS), and spark-assisted compression ignition (SACI). In each of these modes, 3 different CA50 phasings were studied such that all 6 fuels could be studied at the same phasings. Three of the six different fuels used were specially formulated in a previous investigation to study the impact of fuel distillation and aromatic content while maintaining the research octane number (RON) and octane sensitivity. Additionally, neat isooctane and two ethanol containing fuels (RD5-87 and Co-Optima E30) were studied. Different fuel and phasing impacts on emissions were observed across the three combustion modes. Fuel properties were found to impact soot PM and particle number more than the CA50 phasing, while the phasing had more impact on NOx emissions. The NOx emissions were reduced in the PFS mode for all fuels compared to SI combustion, but the SACI combustion mode did not reduce NOx emissions. Although PFS produced low soot PM emissions like SI, total PM mass emissions were significantly higher due to large organic carbon (OC) PM mass contribution. Both PFS and SACI had greater particle number emission than SI operation with small nuclei mode particles dominating in PFS compared to large agglomeration particles in SACI.

1. Introduction

The U.S. Department of Energy's Co-Optimization of Engines and Fuels (Co-Optima) initiative has been pursuing the development of higher efficiency engines by co-optimizing combustion technologies with bio-derived fuel properties. Conventional spark ignition (SI) gasoline engines have been continually improved for better performance and fuel economy since SI engine vehicles were introduced [1], with the first fuel economy standards in the United States passed in the Energy Policy Conservation Act of 1975 [2]. However, their efficiencies are still lower than diesel compression ignition (CI) engines, and like diesel, still require emissions control systems. Fuel-lean, SI gasoline engine operation has been shown to enhance engine efficiencies by reducing throttling losses, heat transfer losses to the coolant, and increasing cyclic work output as a result of increasing specific heat ratio. However, both NOx and particulate emissions are still challenging for fuel-lean SI engines. Fuel-lean exhaust prevents the use of a three-way catalyst (TWC) to reduce NOx emissions because the chemistry requires stoichiometric conditions. High levels of particulate matter (PM), caused by the fuel-rich regions of stratified charge combustion strategies have not yet been resolved [3,4]. Advanced compression ignition (*ACI*) combustion strategies encompass another approach to lean operation where similar

* Corresponding author.
E-mail address: mosesmj@ornl.gov (M. Moses-DeBusk).

https://doi.org/10.1016/j.fuel.2022.125641
Received 23 March 2022; Received in revised form 8 August 2022; Accepted 13 August 2022
0016-2361/© 2022 The Authors. Published by Elsevier Ltd. This is an open access article under the CC BY-NC-ND license (http://creativecommons.org/licenses/by-nc-nd/4.0/).

or improved thermal efficiency benefits can be realized, but where low temperature combustion (LTC) is achieved such that NOx emissions are substantially suppressed. Operational range limits are a challenge for *ACI* modes, especially at high loads, since intense and rapid combustion can result in high pressure rise rates, combustion noise, and potential for engine damage [5,6].

One of Co-Optima's research focuses has been on optimizing multi-mode combustion strategies and fuel properties to achieve increased efficiency and meet emission standards. Multi-mode engines use two or more different engine modes; light-duty (LD) applications typically include conventional SI mode and an *ACI* mode, to increase fuel economy and decrease emissions. Multi-mode operation is a complementary approach for *ACI* operation to overcome its operational restriction at the high load range where *ACI* strategies are limited by relying on SI operation at those loads. While SI can be effectively operated across the entire engine operating map, its comparatively lower air–fuel ratio (i.e., lambda, λ) introduce throttling losses and other thermodynamic inefficiencies.

The drastically different exhaust condition of SI and *ACI* create a challenge in selecting an emission control system for a multi-mode engine. The conventional LD, SI system use TWCs which can efficiently convert CO, NOx, and hydrocarbons (HC) emissions at temperatures between 400 and 800 °C in near stoichiometric conditions. However, the lower exhaust temperatures of *ACI* strategies and excess oxygen limit the efficacy of a TWC, especially the reduction of NOx. The efficiency of a TWC rapidly drops as λ exceeds the stoichiometric point [7]. Emissions control for diesel engines, which also operate lean, rely on an oxidation catalyst (OxyCat) to convert CO and HCs and an ammonia selective catalytic reduction (NH_3-SCR) catalyst to convert the NOx. The catalytic oxidation of HCs over both TWCs and OxyCats have been shown to vary for different hydrocarbon species in stoichiometric and lean conditions [8,9]. Since *ACI* modes typically run at a lean condition, using a conventional TWC for a multi-mode engine may not be able to maintain acceptable NOx emissions reduction over an entire SI/*ACI* operating map [10].

ACI operations for gasoline direct injection (GDI) strategies can be categorized based on the air/fuel stratification: Homogeneous charge compression ignition (HCCI), partial fuel stratification (PFS), moderate fuel stratification (MFS), and heavy fuel stratification (HFS). The fuel stratification can be controlled by fuel injection timing and the fraction of injected fuel at each injection event [11]. PFS operation can be achieved by premixing a fraction of the fuel with the air using port fuel injection or very early direct injection. PFS combustion typically results in higher CO and HC emissions compared to MFS and HFS but results in lower NOx and soot PM emissions.

Another *ACI* operation mode is spark-assisted compression ignition (SACI). This strategy utilizes a spark plug to initiate flame propagation that increases the temperature of the unburned charge triggering auto-ignition. SACI combustion typically results in a reduced peak pressure because a portion of the fuel is consumed by flame propagation rather than autoignition, which is comparatively much faster, and because the control of spark ignition with SACI allows combustion to be phased later, when the combustion chamber volume is higher. As a result of the reduced peak pressure rise rate, SACI can provide a wider range of operation compared to HCCI, but it has shown higher NOx emissions, especially at high load, because it cannot operate as fuel-lean as HCCI due to the requirement to propagate a flame front, resulting in higher combustion temperatures [12,13].

ACI operation with gasoline-range fuels has been shown to greatly reduce NOx and PM emissions compared with diesel-range fuels because of higher volatility and longer ignition delay which provide more time for fuel and air mixing [14–16]. Soot PM formation in GDI engines is known to be formed by the locally poor mixing and wall wetting of fuels which is closely related to engine design and operating conditions such as spraying fuels into the cylinder walls or fuel injection timing [17]. Fuel properties are also an important factor that can impact PM emissions. Particulate Matter Index (PMI), calculated based on the double bond equivalent and vapor pressure of each fuel hydrocarbon species [18], has been used to predict PM emissions dependency on the fuel properties [19]. PMI works reasonably well on predicting soot PM emissions for SI engines under stoichiometric conditions, however, it has shown difficulties in predicting soot PM trends between oxygenated and non-oxygenated fuels [2,20]. It struggles to predict PM trends under different engine operating conditions such as a lean stratified SI engine since PMI only takes fuel chemistry into account [20]. It is also questionable if PMI can predict PM emission tendencies for *ACI* engines which also have lean and/or stratified conditions.

Over the last decade, computational and experimental studies have investigated impacts of operating parameters [21,22] and gasoline-range fuel properties [23–25] on *ACI* combustion. There are a few recent studies in the literature that investigated fuel impacts on engine emissions for *ACI* operation. Zhang et al., investigated the impact of six different physical fuel properties on soot emissions under *ACI* operations at medium load condition using computational fluid dynamics (CFD) and found fuel density to be the only physical property with a notable impact on soot emissions among the six different fuel properties studied [26]. Badra et al., studied effects of eight physical fuel properties on performance and emissions of *ACI* engines at low and high load conditions using CFD [27]. Their models suggested that there are more physical properties that affect *ACI* engine performance and emissions at low load compared to high load. However, the physical property that Badra et al., found the most influential in both low and high load was fuel density. Recent studies in our lab have experimentally investigated the impact of fuel properties and fuel stratification effect on HC and PM emissions from multi-cylinder *ACI* combustion. One study which investigated the impact of fuel aromatic content and distillation range, correlated some of the performance and emissions results to fuel density [28]. However, the measured soot formation did not increase linearly with increasing fuel density likely due to the fact that fuel density cannot be an experimentally isolated parameter. Another study, which speciated the PM emissions into elemental carbon (i.e., soot PM) and organic carbon (OC PM), found that the PM under the more premixed gasoline compression ignition (GCI) modes were dominated by OC PM and both fuel and *ACI* combustion conditions impacted PM across all air–fuel stratifications [29].

An *ACI* engine relies on the auto-ignition of the pre-mixed fuel and air for combustion while a SI engine should avoid it. Therefore, fuel property impacts on engine efficiencies and emissions may differ for SI and *ACI* combustion. A multi-mode engine uses the same fuel for these two different operation modes; hence, it is important to investigate optimal fuels for multiple engine configurations to exploit an optimized engine performance as well as minimize emissions.

In this study, we focused on investigating gaseous and PM emissions from six different fuels across three different combustion strategies (SI,

Table 1
Engine geometry.

Displacement *[liters]*	0.550
Bore × Stroke *[mm]*	86.0 × 94.6
Connecting Rod *[mm]*	145.5
Compression Ratio	12.5: 1
Cam Phasing	Hydraulic cam phaser, 60 CAD authority for intake and exhaust
Fuel Injector	Centrally-mounted solenoid GDI, 8-hole, symmetric 60° included angle

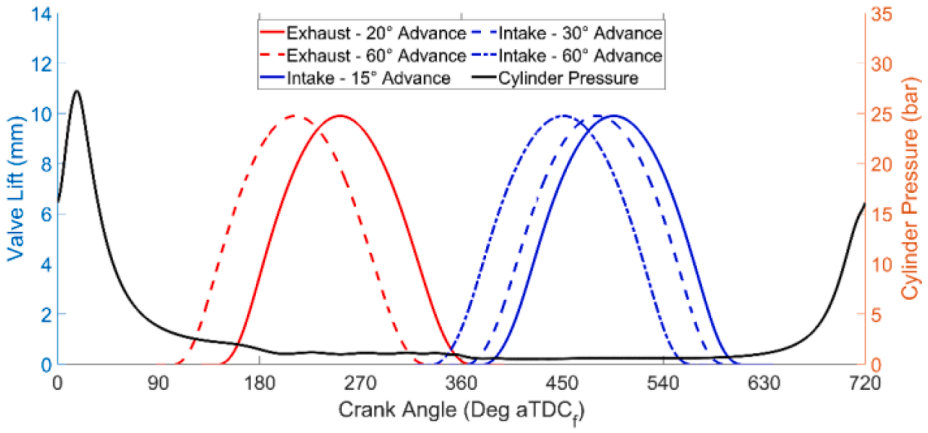

Fig. 1. Intake and exhaust valve timings as a function of cam advance.

Table 2
Engine operating conditions.

	Part-load SI	SACI	PFS
Engine Speed *[RPM]*	2000	2000	2000
gross IMEP* *[kPa]*	474–509	512–540	541–551
Air flow *[g/min]*	235	465	700
Global lambda *[λ]*	1.0	2.0	3.0
Intake Temperature *[°C]*	35	53–85	145–177
Intake Pressure *[kPa]*	61 ± 2	116 ± 2	165 ± 6
Spark Advance *[°CA bTDC$_f$]*	16.5 to 5.6	31.3 to 26	–
Start of Injection 1st/2nd *[°CA bTDC$_f$]*	280/–	280/35–30	280/110–73
Injection Split 1st/2nd *[% injection duration]*	100/–	70/30	70/30
CA50 Criteria *[°CA aTDC$_f$]***	Adv Base Ret 11.8° 15° 20°	Adv Base Ret 0° 3° 6°	Adv Base Ret 7° 8° 10°
Intake/ExhaustCam Advance *[°CA]*	30/20	15/60	60/60
Estimated Residual *[mass %]*	5.4–6.0	14.3–14.6	12.7–12.8

**IMEP: Indicated Mean Effective Pressure.*
***Adv = advanced; Base = baseline; Ret = retarded.

SACI, and PFS) on the same single-cylinder engine designed for multi-mode combustion operation. Additionally, three different CA50 phasings were chosen for each engine strategy such that all six fuels could be operated at the same CA50 phasings. Three of the fuels are what were also used in the previous multi-cylinder *ACI* study [28] from our lab that investigated impacts of the fuel aromatic content and distillation curves on the emissions. In addition to these three fuels, two ethanol containing fuels and isooctane reference fuel were also studied.

2. Experimental section

2.1. Engine setup and operation

This investigation was conducted using a specialized Ricardo Hydra single-cylinder research engine intended for multimode operation, see Table 1 for engine geometry. The engine is equipped with a cylinder head having a four valve per cylinder pentroof design and a centrally-mounted GDI injector. The engine is outfitted for multi-mode operation, so that it can operate under both SI and *ACI* combustion strategies. The PFS, SACI combustion modes chosen for this investigation depend on compositional stratification and high levels of residual trapping in order to properly operate. The necessary levels of stratification are created by injecting fuel twice per cycle, consisting of an early injection and a later injection that is closer to top-dead-center (TDC) firing. The engine is also equipped with hydraulic cam phasers on the intake and exhaust cams, each with a control authority of 60° crank angle (CA), enabling positive valve overlap for SI operation and high levels of residual trapping with negative valve overlap for *ACI* operation. The cam positions used in this set of experiments are shown in Fig. 1. Oil and coolant temperatures were also held fixed at 90 °C for the different combustion strategies in this investigation.

Airflow to the engine was controlled by regulating compressed shop air through an Alicat PCR3 laminar flow element mass flow controller. The intake air was then heated to the required manifold temperature upstream of the intake surge tank. The target manifold temperature and intake heating requirements varied by fuel and operating strategy, see Table 2 for additional information. The intake was also equipped with a tumble plate blocking the lower 54 % of the intake port to increase tumble flow within the cylinder. High-speed intake manifold pressure measurements were made with a Kistler 4049A pressure sensor. The exhaust was open to ambient, with an ECM 5230 EGR meter and wideband oxygen sensor providing the primary lambda measurements. Additional lambda calculations are made with exhaust emissions measurements as a backup to the oxygen sensor. The engine was equipped with the stock ignition coil from a GM 2.0 L LNF engine and an NGK iridium spark plug that is indexed such that the ground strap did not block the fuel spray. The spark dwell was set to 3 ms for SI and SACI operation.

In this study, fuel was supplied to the engine by means of a pressurized piston-style hydraulic accumulator from Parker (Part number A4N0347D1E) with a capacity of 1.5 gallons. The accumulator was pressurized to 110 bar using nitrogen and the fuel pressure is subsequently regulated down to 100 bar with a Tescom (Model number 26-2064V24A27016) fuel pressure regulator. Fuel flow was measured downstream of the regulator with a Coriolis-type flowmeter (Micro-motion model CMF010). The pressurized fuel was then fed into a fuel rail mounted on the engine to damp out pressure oscillations, prior to being fed to a centrally-mounted Bosch solenoid fuel injector. The injector has an 8-hole nozzle with a symmetric spray pattern and 60°included angle.

A National Instruments Powertrain Control Platform was used for both engine control and data acquisition. High speed measurements of cylinder pressure, intake pressure, intake and exhaust cam position, and spark discharge were made with a 0.1°CA resolution for 300 consecutive cycles. Cylinder pressure was measured using a Kistler 6125C pressure sensor and pegged to the high-speed intake pressure measurement for each cycle over a 10° CA window centered at 180° CA before firing TDC (bTDC$_f$). Combustion analysis was performed with a custom-developed Matlab script that computes heat release on a first-law basis [30]. Heat transfer for SI and SACI operation was provided by the Woschni correlation [31] and with the modified Woschni correlation proposed by Chang et al., [32] for PFS operation. Residual trapping was estimated by taking the average of the method by Yun et al., [33] and the state estimation method [34]. The method proposed by Fitzgerald et al., [35] was

Table 3
Select fuel properties.

	Isooctane	LA-LD	LA-HD	Co-Optima E30	RD5-87	HA-HD
PMI	0.19	0.55	1.26	1.28	1.71	2.16
YSI	61.7	64.0	80.0	47.9	83.6	121.8
RON*	100	89.7	90	97.4	92.3	89.6
Sensitivity‡‡	0	4.6	4.6	10.8	7.7	6.1
Aromatic** *[vol%]*	0	6.9	8.1	8.1	23.8	26.3
Olefins** *[vol%]*	0	6.0	5.2	5.0	5.9	5.9
Saturate** *[vol%]*	100	87.1	86.7	57.1	47.4	67.8
Ethanol** *[vol%]*	0	0	0	30.6	9.1	0
IBP† *[°C]*	99.3	33.4	31.8	35.7	40.4	34.3
T50† *[°C]*	–	87.3	118.7	74.3	101.3	129.2
T90† *[°C]*	–	122.9	172.7	155.2	157.9	172.4
FBP† *[°C]*	99.3	160.7	198.4	204.4	205.0	194.3
LHV†† *[MJ/kg]*	44.31	44.17	43.92	38.17	41.93	43.22
AFR$_{stoich}$‡‡	15.14	14.88	14.81	12.92	14.05	14.60
LHV‡‡ *[MJ/kg-air]*	2.93	2.97	2.97	2.95	2.98	2.96
Density‡ *[g/mL, @ 15 °C]*	0.6962	0.7116	0.7383	0.7527	0.7496	0.7630

* ASTM D2699; ** ASTM D81319; † ASTM D86; †† ASTM DD240; ‡ ASTM D4052; ‡‡ calculated values.

also included in the average for PFS and SACI due to their high levels of negative valve overlap. Calculations were made on an individual cycle basis but are reported as data ensemble averaged over all 300 cycles.

2.2. Engine combustion modes

In addition to conventional SI combustion, two advanced combustion modes, SACI and PFS, were explored for this study. Three different crank angles of 50 % mass fraction burned (CA50) were run for each combustion mode: an advanced phasing, a baseline phasing, and a retarded phasing. An overview of the operating conditions for each combustion mode are provided in Table 2 and a summary of the operating procedure for each combustion mode are given below. It should also be noted that the intake pressure levels were not controlled and varied for each fuel under the two *ACI* modes due to differences in intake temperature.

2.2.1. Spark ignited (SI) operation

For SI operation, airflow was set to 235 g/min with the intake and exhaust cam advances set to 30° and 20° respectively. The corresponding cam locations and valve timings are shown in Fig. 1. A single fuel injection event with a start of injection (SOI) timing was set to 280° CA before TDC firing (bTDC$_f$) to approach homogeneous conditions. Airflow and intake temperature were fixed, and fuel flow was adjusted to maintain stoichiometric conditions, or $\lambda = 1$, as the fuels were changed. An overview of these conditions is provided in Table 2. A combustion phasing sweep was first performed with RD5-87 to establish a retarded, base, and advanced combustion phasing. The base and retarded phasings were chosen as 15° and 20°CA after TDC firing (aTDC$_f$), respectively. The advanced combustion phasing was set at 11.8°CA aTDC$_f$ due to RD5-87 reaching the knock-limited spark advance (KLSA), defined as an average peak-to-peak knocking intensity of 25 kPa for a 100-cycle moving average. The remaining fuels were run at the same phasings. The only exception was the HA-HD fuel reaching the KLSA at a combustion phasing of 11.8°CA aTDC$_f$.

2.2.2. Partial fuel stratification (PFS) operation

For PFS operation, airflow was set to 700 g/min and fueling adjusted with an injection split of 70 %/30 % of the total injection dwell until a global lambda of 3.0 was achieved. The first injection was timed at 280°CA bTDC$_f$ and an initial second injection timing of 110°CA bTDC$_f$. The advance on the intake and exhaust cams were both 60°, shown in Fig. 1, resulting in a high level of negative valve overlap and residual trapping. Intake temperature was adjusted on a per-fuel basis until a CA50 timing of 10°CA bTDC$_f$ was achieved, representing the retarded case. Combustion was advanced to the base phasing 8°CA bTDC$_f$ CA50 by retarding the timing of the second injection and increasing the level of fuel stratification. The second injection was further retarded to reach a timing of 7°CA bTDC$_f$ CA50 for the advanced case or until the pressure rise rate (PRR) limit of 10 bar/°CA was reached, whichever came first.

2.2.3. Spark-Assisted compression ignition (SACI) operation

For SACI operation, airflow was set to 465 g/min and maintained for each fuel. Two injections were used to create fuel stratification, one timed at an SOI of 280°CA bTDC$_f$, and a second with variable timing, but initially timed at 30°CA bTDC$_f$. Fuel was adjusted until a global lambda of 2.0 was achieved, while maintaining an injection split of 70 %/30 % of the total injection dwell. The spark was initially timed at 26°CA bTDC$_f$ but was subsequently moved to maintain a delay of 4°CA with the 2nd injection SOI. The delay between the 2nd injection and spark was to ensure adequate fuel stratification for reliable spark-ignition under a globally fuel-lean environment. Intake and exhaust cam advances were set to 15° and 60° to enable negative valve overlap, seen in Fig. 1, and high levels of residual trapping. The intake temperature was increased for each fuel until the timing the 50 % burn timing (CA50) was 6°CA bTDC$_f$, representing the retarded phasing. The 2nd injection and spark timings were then advanced to a base phasing of 3°CA, and the advanced phasing of 0°CA.

2.3. Fuels

A set of 6 fuels with a range of different properties were tested at each operating mode. Three of the fuels were also used in a previous *ACI* study from our laboratory that investigated effects of different distillation and aromatic contents in fuels: Low aromatic low distillation (LA-LD), low aromatic high distillation (LA-HD), and high aromatic high distillation (HA-HD) [28]. The remaining three fuels included the standard reference fuel, 100 % isooctane, and two fuels with different ethanol contents, 10 and 30 %. The 10 % ethanol fuel was the research gasoline known as RD5-87, and the 30 % ethanol fuel was Co-Optima E30, a specially formulated fuel used in many studies across the different laboratories involved in the US DOE Co-Optima initiative. The properties of the 6 fuels are described in.

Table 3 and listed in the order of PMI values throughout this paper.

Yield Sooting Index (YSI) is a measure of the amount of soot a fuel produces when it is doped into a laboratory-scale non-premixed flame [36]; thus, it quantifies a fuel's tendency to form soot solely due to its chemical composition. YSI serves the same purpose as the double bond equivalent term included in PMI, but it can be measured empirically and does not depend on assumptions about the relationship between composition and sooting tendency. The raw values are re-scaled such that YSI ≈ 100 for benzene and YSI ≈ 0 for a fuel that produces no soot.

Table 4
Criteria emissions mass rates measured by FTIR (NOx and CO) and FID (THC) for six fuels in SI, PFS and SACI combustion modes. Mass rates for each fuel-mode combination are reported at 3 CA50 phasings.*

	Isooctane			LA-LD			LA-HD			Co-Optima E30			RD5-87			HA-HD		
	Spark Ignited (SI)																	
	Adv	**Base**	**Ret**	**Adv**	**Base**	**Ret**	**Adv**	**Base**	**Ret**	**Adv**	**Base**	**Ret**	**Adv**	**Base**	**Ret**	**Adv**	**Base**	**Ret**
NOx *[mg/min]*	476	387	269	526	403	283	548	421	290	462	350	239	561	408	280	549	456	326
CO *[g/min]*	0.71	0.69	0.65	0.82	0.83	0.78	0.57	0.64	0.59	0.72	0.77	0.73	0.71	0.70	0.73	0.63	0.68	0.59
THC *[mg C1/min]*	276	257	236	240	223	185	288	277	247	244	229	199	259	239	209	282	275	248
	Partial Fuel Stratification (PFS)																	
	Adv	**Base**	**Ret**	**Adv**	**Base**	**Ret**	**Adv**	**Base**	**Ret**	**Adv**	**Base**	**Ret**	**Adv**	**Base**	**Ret**	**Adv**	**Base**	**Ret**
NOx *[mg/min]*	7.53	5.28	1.86	6.80	4.18	1.61	5.62	3.95	1.29	5.78	3.90	1.57	6.36	4.06	1.33	6.05	3.67	1.45
CO *[g/min]*	0.78	0.85	1.07	0.96	1.04	1.46	1.03	1.13	1.44	1.01	1.04	1.41	1.16	1.19	1.57	1.12	1.27	1.65
THC *[mg C1/min]*	532	557	622	536	570	642	560	591	667	522	563	659	561	581	666	563	589	682
	Spark Assisted Compression Ignition (SACI)																	
	Adv	**Base**	**Ret**	**Adv**	**Base**	**Ret**	**Adv**	**Base**	**Ret**	**Adv**	**Base**	**Ret**	**Adv**	**Base**	**Ret**	**Adv**	**Base**	**Ret**
NOx *[mg/min]*	575	456	331	533	418	344	528	414	334	522	422	311	533	427	331	517	407	313
CO *[g/min]*	0.42	0.59	1.19	0.47	0.68	0.97	0.46	0.65	1.02	0.52	0.73	1.37	0.48	0.64	1.04	0.52	0.73	1.25
THC *[mg C1/min]*	470	551	875	467	509	651	474	503	628	459	512	817	460	493	644	491	529	681

CA50 phasings: Advanced (Adv), Baseline (Base), Retarded (Ret)

The values reported in Table 3 were measured in this study except for isooctane, which was taken from an extensive compilation of YSIs measured for pure compounds [37], and Co-Optima E30, which was taken from an earlier study of Co-Optima gasolines [36]. The procedures used for the new measurements were identical to those described in Ref. [36].

2.4. Emissions sampling setup

2.4.1. Gaseous emissions

Multiple gaseous emissions measurements are taken during multi-mode operation. Standard criteria emissions were measured using both a standard 5-gas emissions bench analyzers from California Analytical Instruments (CAI) and a fast 5 Hz, MKS FTIR. The sampling locations were upstream of the exhaust surge tank with the exhaust gases drawn through heated filters. The heaters and transfer lines were kept at 191 °C to prevent condensation of the water in the exhaust. The only CAI bench analyzer data reported was from the total unburned hydrocarbons (THC) which were measured with a heated flame ionization detector (Model 700-HFID). All other criteria emissions and hydrocarbon speciation reported were collected by FTIR.

2.4.2. Particulate matter (PM) emissions

An AVL MicroSoot Sensor (MSS) that is based on a photoacoustic measurement method was used with the associated AVL heated sampling line to measure soot emissions. Similar to the MSS, additional, PM emissions were sampled using 45° sampling probes placed in the exhaust pipe upstream of the exhaust surge tank. The additional PM sampling transferred exhaust to dilution systems using Entech heated (191 °C) sample lines. All dilutions were made with compressed and dried air after a three-stage filtering system. One probe sent exhaust to a single dilution tunnel using an ejector pump and filtered air. After dilution, the exhaust was maintained at ~ 47 °C.

The single dilution tunnel was used for collecting PM on filters for mass measurement. Filter sampling and analysis has been previously described [38]. Briefly, gravimetric PM mass was collected on Whatman, $PM_{2.5}$ PTFE 47 mm filters. The elemental carbon (EC) and organic carbon (OC) speciation of PM was performed by collecting PM samples on pre-fired quartz fiber filters. The PM laden quartz fiber filters were sent to Sunset Laboratory, Inc. for EC/OC determination by the NIOSH method [39]. All primary quartz fiber filters were corrected for known filter adsorption artifacts of HC using an adsorbed organics measured on secondary quartz fiber filters collected behind a PTFE filter in parallel with the primary quartz fiber filter [40]. The PM at each conditions studied was analyzed for EC/OC PM mass as just described while the gravimetric PM mass was measured in our lab for each fuel-mode condition at the baseline CA50 phasing.

A second probe was used to for particle number (PN) and size distribution sampling. The heated sampling line directed the exhaust to a two-stage dilution system before being sampled by a TSI Engine Exhaust Particle Sizer (EEPS; TSI model 3090). The two-stage dilution system design was based on an ejector pump design similar to the European Particle Measurement Programme (PMP) [41]. The in-house built system has been previously reported [29]. Briefly, the exhaust was diluted with 150 °C thrice filtered air, then sent through a 350 °C evaporation tube section before the second dilution with thrice filtered air. The doubly diluted exhaust is then sent through a 50 °C section before being sampled by the EEPS. The EEPS measured the concentration of both the total Particle Number (PN) at 10 Hz and size distribution of the particles with a 16 channel per decade resolution. All data presented was normalized ($dN/dlogD_p$), corrected for dilution and converted from volumetric concentrations (#/cm^3) to a rate (#/min) using the volumetric flow rate (cm^3/min) to allow for a more direct emissions comparison between fuels and operating conditions.

3. Results and discussions

The gaseous and PM emissions were converted to mass rates for the best comparisons between different combustion modes, as a result of the different mass flow rates that occurred due to different lambdas used in each mode. The results are separated into gaseous and PM emissions with subsection in each focused on the impact of fuel and CA50 phasing within each mode (SI, PFS and SACI). Data for all modes will be presented together the first time it is referenced to enable easy comparison, but the fuel effects will be discussed in respective modes.

3.1. Gaseous emissions

3.1.1. SI mode

In the conventional SI mode, the CA50 phasing had limited impact on emission mass rates, only impacting the NOx criteria emissions, see Table 4. While the NOx emission rates were high across all phasings for

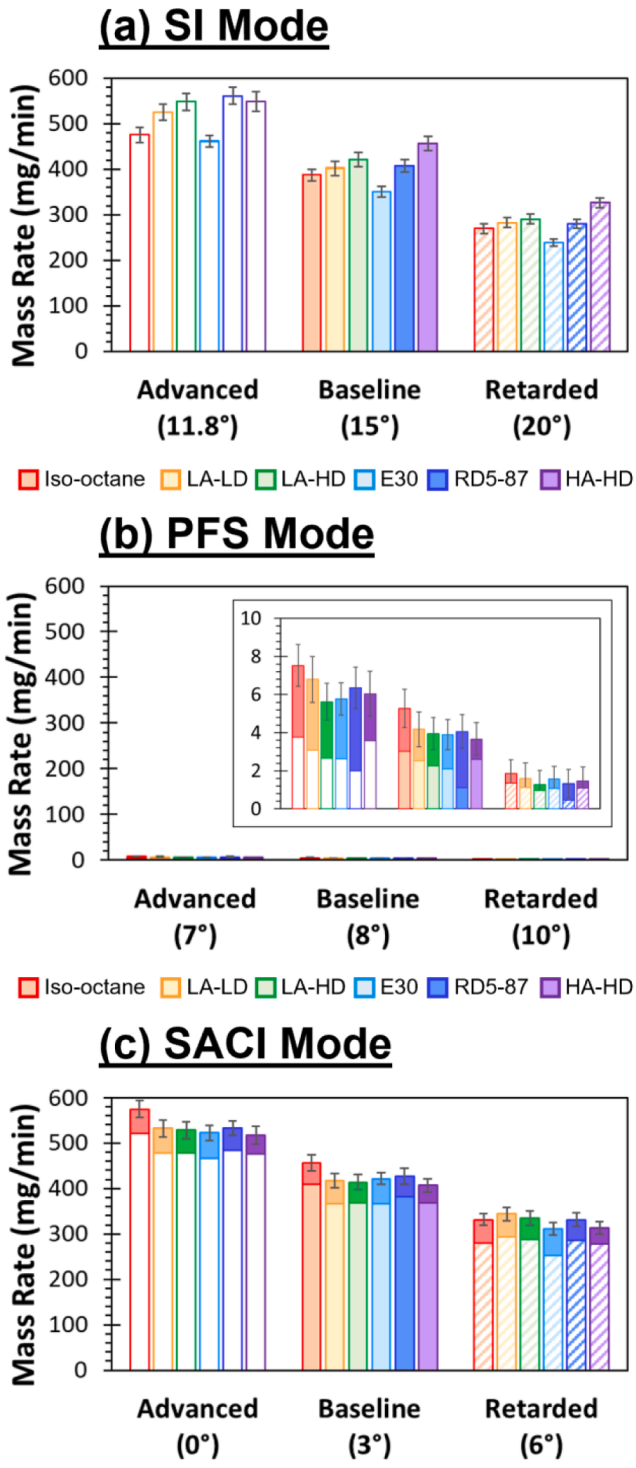

Fig. 2. Fuel impact on NOx emissions from FTIR at each mode-phasing condition studied. The NOx emissions NO (open bars) and NO_2 (solid bars) are shown for all conditions, inset graph magnifies the y-axis ranges. Error bars are standard deviation from total NOx averages.

SI, they decreased as the phasing was retarded. The remaining criteria gaseous emissions also shown in Table 4, CO and total hydrocarbons (THC), were generally low and unchanging as the phasing was retarded. Consistently lower NOx emissions were seen at all phasings for E30 which contained 30 % ethanol compared to emissions from the other fuels, Fig. 2**(a)**, but a similar drop did not occur for RD5-87 which contained 10 % ethanol. At every phasing in the SI mode, NO_2 emission

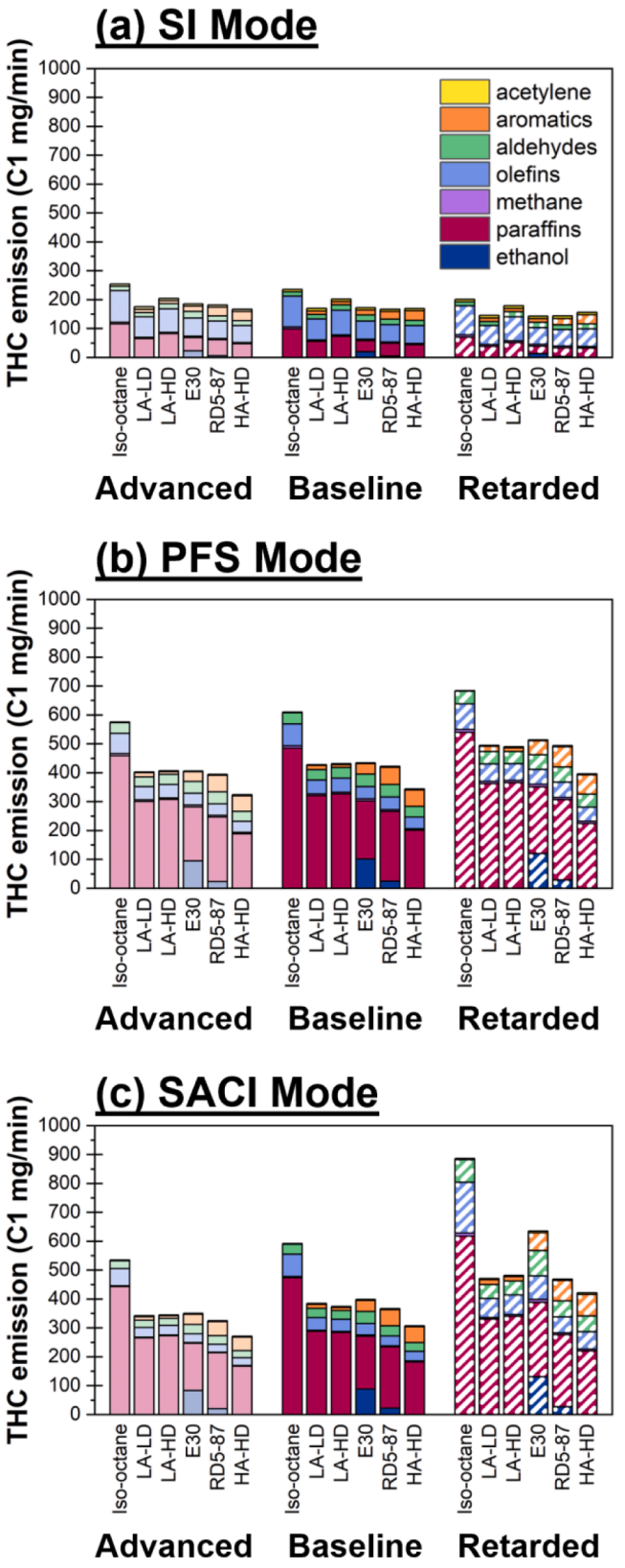

Fig. 3. THC C1 mass emissions with HC speciation by functional group for each mode across advanced, baseline and retarded CA50 phasing conditions. Species were identified by FTIR method and summarized into ethanol, paraffins, methane, olefins, aldehydes, aromatic, and acetylene.

were negligible such that the NOx emissions consisted almost exclusively of NO.

The SI mode THC emissions measured by FTIR are shown in Fig. 3**(a)** and in good agreement with FID values shown in Table 4. Speciation of HC emissions chemical functionality by FTIR provides a more detailed look at how engine operation and fuel impacted emissions including oxygenated species, for which a FID struggles to accurately measure. The results shown in Fig. 3 simplify the FTIR speciation measurements by grouping the HCs based on their chemical functionality. While parafins and olefins are the major types of HCs emitted for all fuels in the SI mode, the two higher aromatic fuels, RD5-87 and HA-HD, showed an increase in aromatic HC emissions at all three phasings compared to the other fuels. The amount of methane and aldehydes in the exhaust were relatively consistent over all six fuels and across all phasings.

3.1.2. PFS mode

Combustion phasing can influence engine emissions due to its impact on in-cylinder temperatures. Comparing the PFS trends in Table 4, the NOx emissions increased whereas the CO and THC emissions decreased as the phasing advanced. Saxena et al., observed a similar increase in NOx emissions as combustion timing was advanced in an HCCI engine. An increase of the peak in-cylinder temperature also occurred as combustion was advanced and the equivalence ratio was increased which they attributed to the occurrence of autoignition at a smaller in-cylinder volume which led to a higher in-cylinder pressure [42].

The criteria mass emissions rates in PFS mode for all fuels at each CA50 phasing studied are listed in Table 4. As expected, the low temperature combustion of the PFS mode resulted in low NOx emissions with exhaust concentrations below 10 mg/min at all three phasings. While the PFS mode reduced NOx formation, the trade-off lowered combustion efficiency which resulted in increased CO and THC emissions from unburned and partially burned fuel. The substantial NOx–THC trade-off was seen at each phasing for all fuels at the PFS operating conditions in this study, consistent with other *ACI* studies [43].

Overall, NOx emissions remain low; however, the NO_2/NOx ratio, see Fig. 2**(b)**, was high in PFS mode, especially at the baseline and advanced phasings. The NO_2/NOx ratio is typically small for spark ignition engines, while compression ignition (CI) engines are reported to have higher NO_2/NOx, in the 10 – 80 % range depending on the fuels or engine operations such as engine speed, loads, and EGR [44,45].

The formation of NO_2 during combustion comes mainly from the reaction of NO with HO_2 radicals and hydrocarbons. Under relatively low combustion temperatures, 600 – 1100 K, the promotion of this conversion is dependent on the species of hydrocarbons available [45–49]. Several experimental and modeling studies have shown that while low temperature combustion results in lower NOx emissions the NO_2/NOx ratio is high and that the NO–NO_2 conversion is sensitive to temperature [43,49–52]. Benajes et al., computationally examined NOx emissions and found the combustion process itself could not be responsible for an increase of NO_2 ratio [51]. Later, Yu et al., performed an experimental compression test with CI research engines and confirmed high NO to NO_2 conversion can be reached under certain intake HC/NO ratios [49]. Based on these previous studies, the high NO_2/NOx ratio in the PFS mode may have resulted from low in-cylinder temperatures and the high concentrations of THC emissions.

Slightly higher NOx and lower CO emissions with isooctane fuel can be seen in Table 4, but overall, limited fuel-specific impacts on gaseous emissions in PFS mode were seen. Although no fuel impacts were seen for THC emissions measured by FID, noticeable fuel impacts for THC emissions were measured by FTIR, Fig. 3**(b)**: isooctane was significantly higher than the other fuels while the HA-HD was slightly lower than the remaining fuels. Furthermore, total C1 mass rates measured by FTIR deviated from FID measurements by roughly 100 mg/min for all fuels and across all three CA50 phasings with the FTIR indicating greater THC mass compared to the FID for the isooctane fuel but lower for all of the other fuels.

The FID is a linear detector that can measure ions generated from HCs burning in a hydrogen or oxygen flame and is widely used to measure the gaseous THC in engine emissions. The signals from THC are proportional to the number of carbons in the THC species and reported in terms of a bulk C1 concentration. The FID, however, does not have a linear response to oxygenated HCs limiting its effectiveness at capturing all carbons associated with these types of HC species, such as aldehydes. The C1 mass of aldehydes identified by the FTIR in Fig. 3 for the isooctane fuel closely matches the increased THC mass compared to the FID mass at each CA50 phasing in the PFS mode, suggesting the FID's limited response to oxygenates can largely account for the FTIR-FID difference of this single component fuel.

While the FTIR can speciate many HC species, the large variety of HCs in engine exhaust often limits an accurate analysis of them [53–56]. This limitation is a consequence of overlapping stretching frequencies between multi-chain HCs, making it difficult to resolve all of the species and contributing to misrepresentations in method identification. A study by Southwest Research Institute and General Electric Transportation has shown that while FTIR analysis can detect both butane and octane at the same stretching frequency as propane with a linear response but with varying response factors [56]. Since multiple paraffin species in engine exhaust can contribute to the same stretching frequency that is identified as a single species, it limits the quantitative accuracy attributed to the identified species.

Conversion of a HC concentration measured by FTIR to a C1 mass rate will be impacted by the number of carbons in the HC species used in the calculation. Nearly 80 % of the PFS mode THCs were paraffins, but the FTIR method used in this study only included speciation of ethane (*C*2), isopentane (C5) and cyclohexane (C6) with the majority being reported as C5. The authors hypothesize that some fraction of the paraffins treated as a C5 HC are likely other larger HC species, contributing to the lower FTIR C1 mass rate of the full formulation fuels compared to the FID C1 measurement. There are other reported studies that have shown the THC emissions detected by FTIR underestimate FID results [53–55].

In addition to larger paraffins and aldehydes, other oxygenated species not measured by FTIR may also be contributing to the higher FID C1 rate. In a recent paper by Lewis et al., the researchers detected multiple nitro and carboxylic acid functional HC compounds in organic carbon (OC) collected with a quartz fiber filter [57]. These compounds could also exist in gaseous HC emissions but may not have been detected with the FTIR method or fully accounted for by the FID. Storey et al., compared FTIR THC measurements in a GCI emissions study using a typical gasoline FTIR method and a newly developed LTC method which included more oxygenated species in the calibration [43]. This study demonstrated an increase in HC emission for the same emissions data when using the method which incorporated more oxygenated species.

Regardless of the exact total of the C1 mass rate, comparison of FTIR functional speciation between fuels shown in Fig. 3 suggested that there are some fuel-specific impacts on the HCs present in PFS emissions. The major functional species in the THC emissions were paraffins for all the fuels but off-set some by ethanol emissions proportional to the ethanol content in the RD5-87 and E30 fuels. A significant fraction of aromatics in the RD5-87 and HA-HD fuels compared to the other fuel compositions, see.

Table 3, resulted in greater aromatic HC species in the emissions of these two fuels and was seen across all CA50 phasings. Interestingly, E30 emitted almost 4 times more aromatic HCs than the LA-LD or LA-HD which had similarly low aromatic fractions in the fuel. Burke et al., [58] and Ratcliff et al., [59] have both shown that ethanol in fuels delays the evaporation of heavy aromatics because of increased volatility of mixture and positive azeotrope interaction between ethanol and HC. The delayed evaporation of aromatics could result in relatively poor mixing with air and remain as unburned HCs in exhaust gas. It is probable that the FTIR C1 mass rates for the aromatic contribution shown in Fig. 3

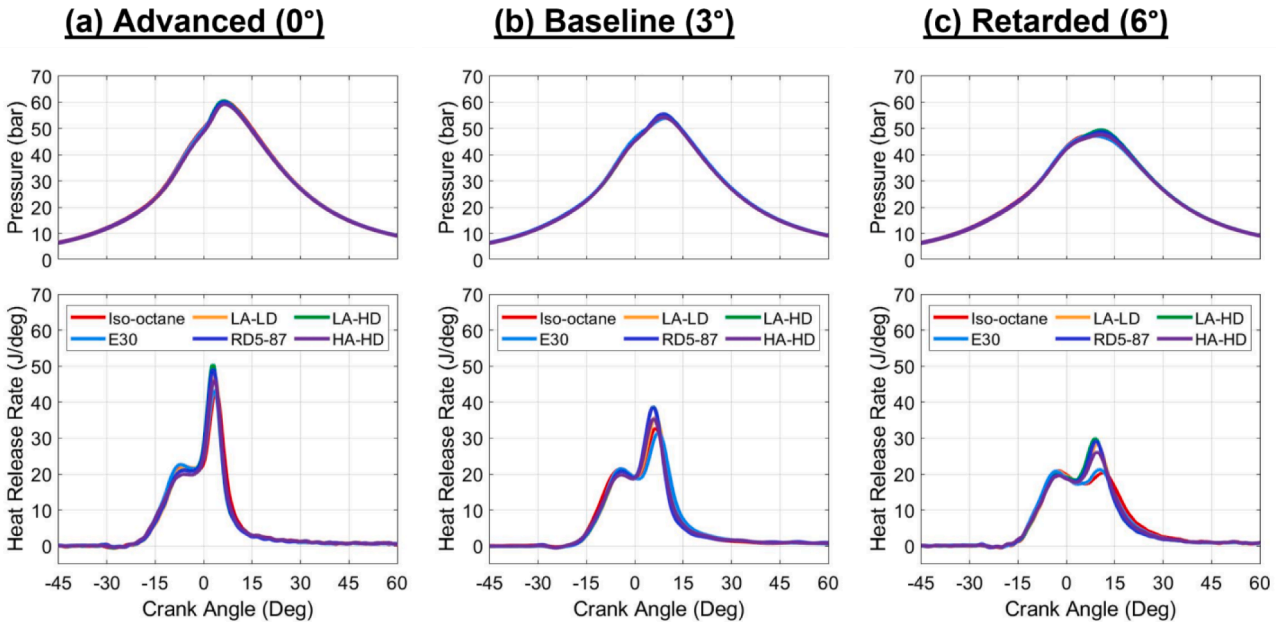

Fig. 4. Pressure and heat release rate for each fuel in SACI mode at the (a) advanced, (b) baseline, and (c) retarded CA50 phasings.

were also underestimated since the FTIR method reported aromatics as a group value identified as "aromatics as C7" and other aromatics, such as xylenes, ethyl benzene, and larger alkylated aromatics, are expected to be present. The aromatic identification along with the paraffins are likely major contributors to the lower C1 mass rate measured by FTIR compared to the FID. Thus, the THC mass rates are expected to be closer to FID mass rates, but the FTIR speciation gives a good first approximation of the distribution of the THC functional speciation.

3.1.3. SACI mode

Similar to PFS combustion, retarding CA50 phasing was found to decrease NOx and increase CO and THC emissions from SACI combustion. Overall, high NOx and THC emissions were observed in SACI operation as shown in Table 4. The highest NO_2 mass rate was seen in the SACI mode for all fuels and phasings, as seen in Fig. 2. While NO_2 emissions were high compared to the other modes studied, it accounted for only a small fraction of the high total NOx emissions in the SACI

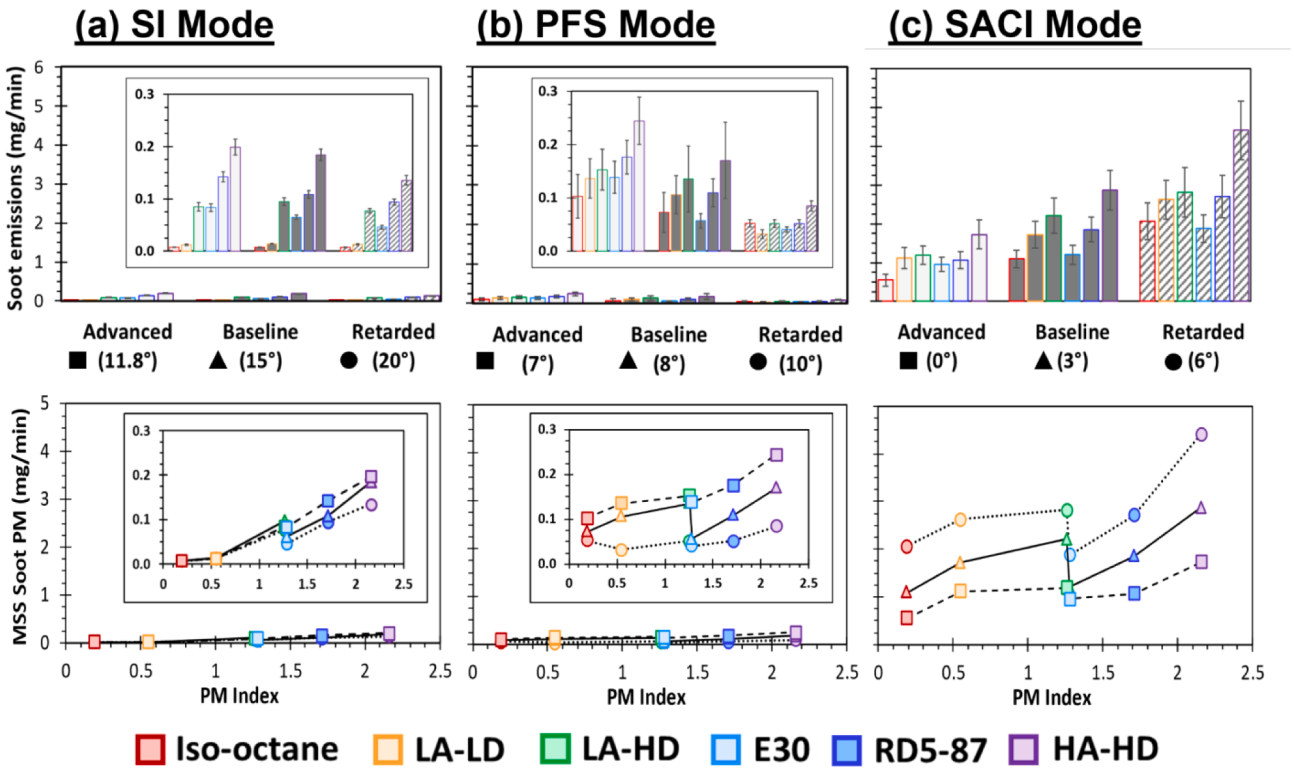

Fig. 5. Top bar graphs show soot PM mass emission rates from MSS measurements for each fuel. Fuels follow increasing PMI left to right and are color coded. Bottom graphs plot soot PM mass rates as function of PMI, lines are just to guide tracking trends. Inset graphs magnify the y-axis ranges. All results are grouped by CA50 phasing: advanced (■, dashed line), baseline (▲, solid line) and retarded (●, dotted line) for each mode SI (a), PFS (b), SACI (c).

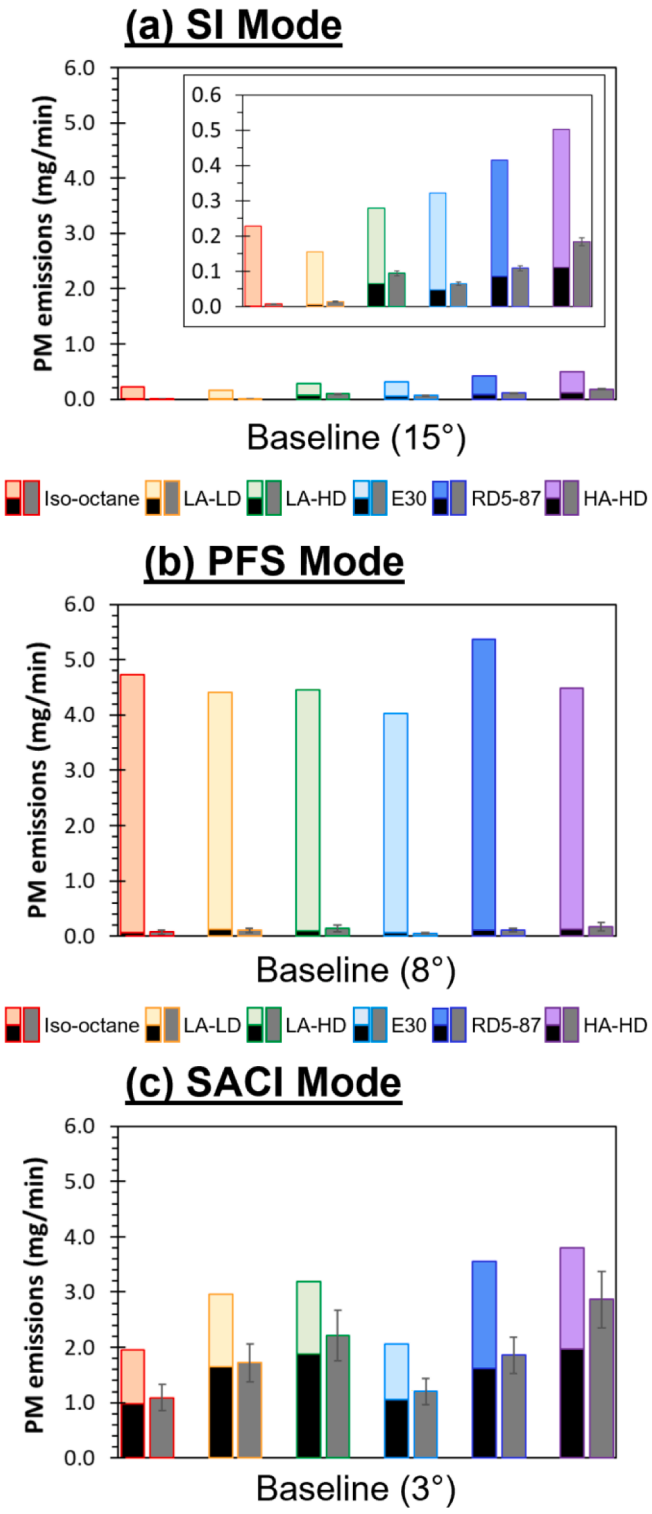

Fig. 6. Total carbon PM mass rates derived from EC/OC analyses are compared to the MSS soot PM rates at the baseline CA50 phasing from Fig. 5 for all fuels in (a) SI mode, (b) PFS mode and (c) SACI mode, inset graph magnifies the y-axis. The stacked bars are EC and OC PM (black and color coded to fuel, respectively) rates, the gray bars to the right of EC/OC are soot PM mass rates from MSS.

mode. An interesting gaseous emissions result in the SACI mode was the appearance of excessive amounts of CO and THC emissions in the retarded phasing for the isooctane and E30 fuels. This was the only distinct fuel-specific impact on criteria emissions observed in SACI mode. The increase in these fuels at the retarded phasing was also captured in the FTIR THC mass rates, Fig. 3**(c)**. While other THC discrepancies between the THC C1 mass rates from FTIR and FID exist in SACI mode, mirroring those discussed for PFS, this unique fuel-specific impact stands out. Speciation by FTIR suggests the fuel specific increase in THC mass rates mainly comes from increased olefins and aldehydes with higher aromatic emissions also contributing for the E30 fuel. The higher CO emissions in combination with increased HC species in the emissions, especially the olefins, support incomplete combustion of the fuel.

The heat release rates plotted in Fig. 4 indicate no notable differences between fuels, except for the significantly lower heat release rate post end-gas autoignition for isooctane and E30 fuels in the retarded phasing. The first heat release rates due to the flame propagation are similar between fuels across all three phasings. Incomplete combustion for isooctane and E30 may stem from insufficient charge stratification levels at the time of the spark event, related to the high volatility of both of these fuels [60]. Interestingly, the isooctane and E30 fuels also have high RONs (100 and 97.4, respectively) while the rest of the fuels have significantly lower RONs in the 90–92 range. Further investigation is needed to better understand this unique emissions behavior at retarded CA50 timings in the SACI combustion mode.

3.2. PM emissions

3.2.1. SI mode

Fig. 5**(a)** shows soot PM emissions measured with an AVL MSS for all fuels at the 3 different CA50 phasings in the SI mode as well as ploting the mass rates against fuel PMI. While SI soot PM emissions were low, an increasing trend within each phasing as the fuel PMI increase was observed in additon to a slight decrease in mass rate as the phasing was retarded. Both ethanol containing fuels (E30 and RD5-87) deviated from a linear correlation between soot PM mass and fuel PMI. The degree of deviation correlated with the fraction of ethanol.

The suggested impact of ethanol was further highlighted by the lower soot PM emissions produced by E30 compare to LA-LD despite their similar PMI values (1.28 vs 1.26, respectively). The disparity in soot PM mass between E30 and LA-LD became more prominent as the CA50 phasing was retarded. Lower soot emissions are typically reported for ethanol containing fuels [2,61–63]. The lower ethanol content and higher aromatic fraction in RD5-87 diminished the soot PM reduction effect compared to E30, but still showed a reduction in comparison to HA-HD which had a similar high aromatic fraction. In the baseline and retarded phasings, RD5-87 produced a similar soot PM mass rate as LA-HD despite its higher PMI value (1.71 vs 1.26, respectively).

In Fig. 6**(a)**, the MSS measured soot PM mass rate at the baseline phasing was compared with the EC/OC PM mass rate. The soot emissions measured by the MSS were slightly higher than the EC mass rate measured for all fuels, but shows the same trends. The total PM also shows an increasing trend as PMI values increase, except for the single component isooctane reference fuel which produced more PM emissions comparitively than the PMI trend would predict.

Cumulative PN emissions rate from each fuel across the different CA50 phasings in SI mode are shown in Fig. 7**(a)**. The total PN emissions follow the same trend as soot PM with PN emissions decreasing slightly as the phasing was retarded and nominally increasing as the fuel PMI value increased. Similar to soot PM mass, the total PN trend dips for the ethanol containing RD5-87 and E30 fuels at all phasings.

The size distributions for the PN rate of all the fuels from the baseline phasing in SI mode are shown in Fig. 7**(a)**, lower graph. The bimodal size distributions seen for all fuels in the SI baseline CA50 phasing were also observed at the advanced and retarding phasings. Lower PN rates were seen at the larger size distributions for the low PMI fuels, isooctane and LA-LD, explaining the significantly lower soot PM mass rates shown in Fig. 5**(a)**.

To better understand how the PM particles correlated with PM mass the EEPS measured PNs were converted to a mass rate and compared

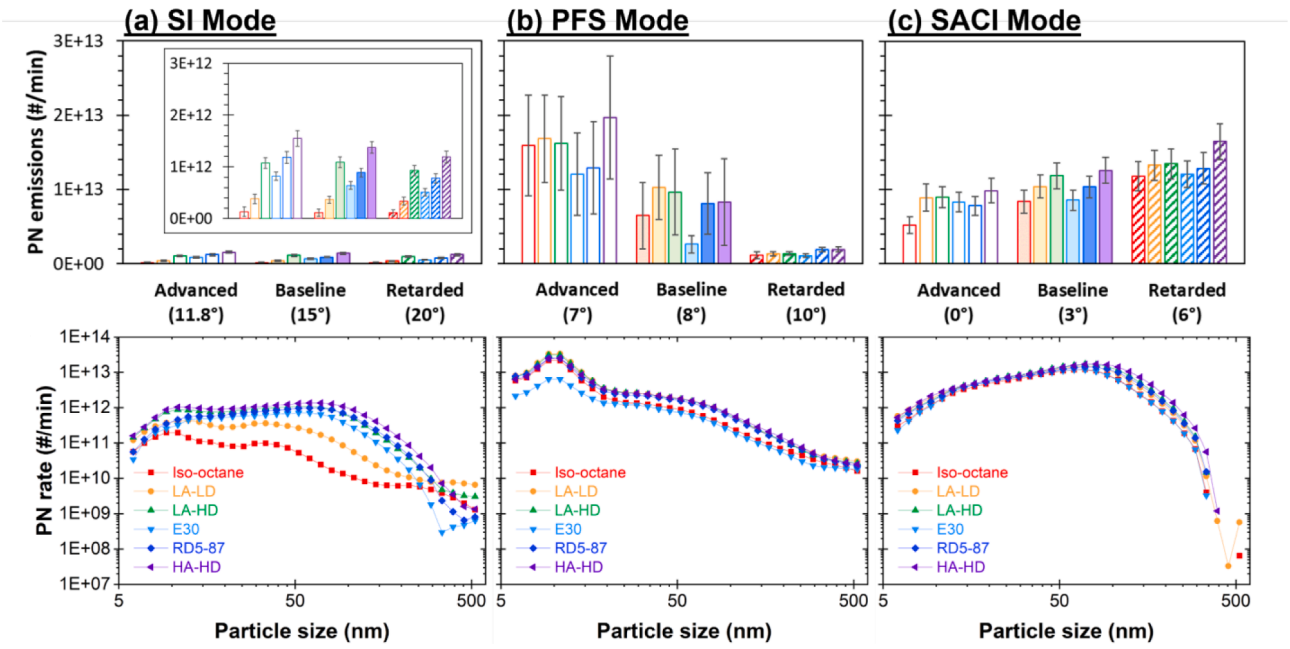

Fig. 7. Top bar graphs show particle number (PN) rates for each fuel and grouped by CA50 phasing within each mode. Bottom graphs plot the PN rate as a function of size distributions for all fuels at the baseline CA50 phasing. The inset graph magnifies the y-axis.

with MSS measured soot PM mass rates. To calculate PM mass from PN measurements, the effective densities were derived from the equation and parameters for GDI and LDD vehicles suggested by Maricq and Xu [64]. A comparison of the SI mass rates derived from the two techniques at 3 different CA50 phasing are shown in Fig. 8**(a)**. The mass rates derived from PN were slightly higher for all fuels in all phasings but correlated well with the MSS mass rates.

3.2.2. *PFS mode*

The soot PM emissions in PFS mode, Fig. 5**(b)**, were at similar mass rates as those seen in the SI mode for all fuels. The highest average soot PM was less than 0.25 mg/min in the advanced phasing and a decreasing trend was observed as phasing was retarded. This may have stemmed from decreasing stratification that resulted as earlier 2nd fuel injections were used to retard CA50 phasing. Soot PM emissions from each fuel generally showed an increasing trend with increasing PMI but were impacted similar to SI soot PM emissions when ethanol was present in the fuel. A more significant deviation from the linear soot PM-PMI correlation for the ethanol fuels was seen at the PFS baseline CA50 phasing compared to the advanced and retarded phasings, suggesting both fuel and the combustion process contributed to this reduced soot PM.

The EC/OC derived PM mass rates in Fig. 6**(b)** were compared the MSS soot PM mass rates for each fuel at the baseline phasing. The EC mass rate was shown to be in good agreement with the MSS soot rate while the total PM mass rates which included OC PM contributions were significantly higher. The low combustion temperatures of the PFS mode which can contribute to the large amounts of unburned CO and THC also likely promoted these high OC PM emissions. The total PM mass emissions which are the combination of EC and OC values do not show any correlation to the PMI number at this PFS mode and displayed little fuel impact.

PN emission rates in the exhaust gas for different fuels at the each CA50 phasing in PFS mode are described in Fig. 7**(b)**. A decrease in PN rate was observed for each fuel as the phasing was retarded correlating with the soot PM mass trend; however, the magnitude of the PN rate reduction from advanced to retarded phasing was more significant. The size distributions of PFS mode particles shown in the lower Fig. 7**(b)** graph for the baseline phasing suggested that high PN but moderate PM reduction was linked to the dominance of smaller nucleation mode particles, below 23 nm of diameter. This skewed size distribution was also seen at the other phasings, and PN decrease as the phasing retards predominately occurred in the nucleation mode particles for each fuel.

The mass rates derived from EEPS PN size distributions compared to MSS mass rates at the each CA50 phasing in PFS mode are shown in Fig. 8**(b)**. The PN mass rates are higher than those from the MSS for all fuels and deviate from the MSS fuel trend. The increased deviation in the mass suggests that either the effective densities for the PFS particles are different than those used and/or some of the OC PM particles were still measured by the EEPS despite the 350 °C thermal denuder section of the double dilution conditioning system. Different effective densities suggested by Xue et al., [65] were also tried, but the values of calculated PM mass only changed about 6 % from those calculated with effective densities proposed by Maricq and Xu [64] used in Fig. 8.

3.3. *SACI mode*

Retarding the CA50 phasing in SACI mode resulted in increasing soot PM emissions for all fuels, Fig. 5**(c)**. The increasing trend may be a result of fuel impingement on the piston that stems from the late 2nd fuel injection near TDC that was used for SACI. The distance between the spray and the piston was closer as phasing was retarded and may have increased the impact of the fuel impingement on soot PM emissions. Similar to SI and PFS modes the ethanol content in E30 and RD5-87 lowered soot emissions compared to fuels with similar or higher PMI values at all CA50 phasings.

In Fig. 6**(c)**, the MSS soot PM mass rates were compared with EC/OC PM mass rate measurements at the baseline phasing and again showed good agreement between MSS soot and the EC PM fraction. The OC PM mass rate for all fuels in SACI mode accounted for about half of the total PM mass rate. The total SACI PM mass rates showed an increasing trend as PMI values increased, except E30. The other ethanol containing fuel, RD5-87, deviated from the PMI trend when only soot PM was considered, but the total carbon PM mass rate followed the trend of increasing PM mass with increasing PMI.

The fuel effect on PN emissions across all three phasings followed the soot PM trend as might be expected for a mode with a significant EC fraction of in the total PM mass, Fig. 6**(c)**. Only a mild dip in PN rate was

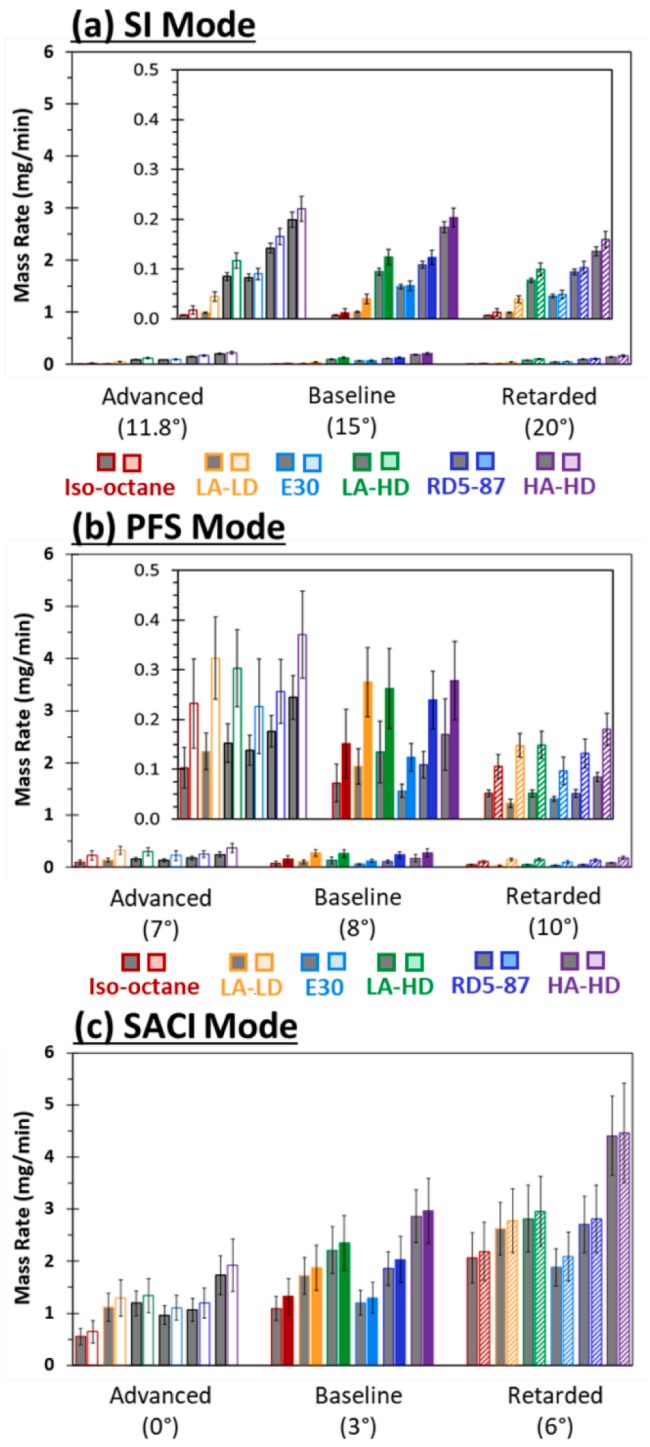

Fig. 8. MSS soot PM mass rates (gray) compared to Particulate mass rate derived from EEPS size distribution (color-coded) for all fuels grouped by CA50 phasing within (a) SI, (b) PFS, and (c) SACI mode. The inset graphs magnify the y-axis ranges.

seen for the two ethanol containing fuels in Fig. 7**(c)**. The overall fuel impact on PN emissions was small at each phasing and PN emissions increased only slightly as the CA50 phasings were retarded. The limited impact on PN emissions between different fuels was also reflected in the size distributions, as shown in lower graph Fig. 7**(c)** for the baseline phasing. The PN derived mass rates at each phasing in SACI mode, Fig. 8 **(c)**, were in good agreement with the MSS mass rates and follow the same fuel trend. The higher EC or soot PM mass fraction of the total PM mass rate seen in the SACI mode supports the strong agreement.

4. Conclusion

As the previous studies have implied, engine emissions are not solely dependent on fuel itself but include engine hardware and operational choices, therefore, integrative consideration is important to develop better engines and fuels. The emission results from this study may be able to provide guidance in the development of an emissions control system solutions for multi-mode engine, and guidance on what fuels and combustion modes may be feasible for emissions compliance.

Different fuel and phasing impacts on emissions were observed across the three combustion strategies: SI, PFS and SACI. While many unique results from this work have been presented, a few notable findings have been summarized:

- Combustion efficiency changes between the three modes had the expected impacts on CO and THC which increased as efficiency dropped. Limited impact from fuel properties and CA50 phasings was seen on most of the mass rate of the gaseous criteria emissions, except NOx emissions.
- The NOx emissions for the PFS combustion mode were approximately 2 orders of magnitude lower than the SI and SACI modes, which were similar. Additionally, fuel-specific differences on NOx emissions were a secondary effect. In all three modes, NOx emissions dropped as the CA50 phasing was retarded. Mode impacts on the NO_2/NOx ratio were notable. Both *ACI* modes generated NO_2 while almost none was measured in the SI mode. For the PFS mode, NO_2 accounted for nearly half of the total NOx at the most advanced phasing. As the total NOx dropped even lower as the PFS phasing was retarded, the NO_2 fraction also diminished. While NO_2 only accounted for around 10 % of the SACI mode NOx, the consistent mass rate of 50 mg/min (±10) for SACI combustion was higher than the mass rate of NO_2 from the PFS combustion mode, regardless of fuel or phasing.
- The *ACI* modes generated a different composition of THC species than the SI mode. Olefins accounted for a significant fraction the THC mass rate in SI mode while the two *ACI* modes were dominated by paraffins and included significant contributions from aromatic and aldehyde species.
- The SACI mode generated an order of magnitude more soot PM emission than the SI and PFS modes. However, when the OC PM fraction was considered, both *ACI* modes had an order magnitude more total PM mass than the SI mode for the baseline phasings measured. The order of magnitude change in the mass rate of the PFS mode was due to the high OC PM emissions.
- The most notable fuel effects were seen for the soot PM mass emissions which were further influenced by the combustion mode and CA50 phasings. The SI and PFS modes both saw a drop in soot PM emissions as the phasing was retarded while the SACI soot PM increased.
- The combustion mode had a notable impact on the size distribution of the particle emissions. The SI mode had a more even bimodal distribution while the PFS mode skewed to the smaller, nuclei mode particles and SACI mode to the larger, accumulation mode particles.

5. Note

This manuscript has been authored by UT-Battelle, LLC, under contract DE-AC05-00OR22725 with the US Department of Energy (DOE). The publisher acknowledges the US government license to provide public access under the DOE Public Access Plan (https://energy.gov/downloads/doe-public-access-plan).

CRediT authorship contribution statement

Yensil Park: Formal analysis, Writing – original draft, Writing – review & editing, Visualization. **Melanie Moses-DeBusk:** Conceptualization, Methodology, Investigation, Writing – original draft, Writing – review & editing, Visualization, Supervision, Project administration, Funding acquisition. **Tommy Powell:** Investigation, Writing – original draft, Writing – review & editing, Visualization. **James Szybist:** Conceptualization, Methodology, Writing – review & editing, Supervision. **Zhanhong Xiang:** Investigation. **Junqing Zhu:** Investigation. **Charles S. McEnally:** Writing – original draft, Writing – review & editing, Supervision, Funding acquisition. **Lisa D. Pfefferle:** Methodology, Supervision.

Declaration of Competing Interest

The authors declare that they have no known competing financial interests or personal relationships that could have appeared to influence the work reported in this paper.

Data availability

Data will be made available on request.

Acknowledgements

This research was conducted as part of the Co-Optimization of Fuels & Engines (Co-Optima) project sponsored by the U.S. Department of Energy (DOE) Office of Energy Efficiency and Renewable Energy (EERE) Bioenergy Technologies and Vehicle Technologies Offices. Co-Optima is a collaborative project of multiple national laboratories initiated to simultaneously accelerate the introduction of affordable, scalable, and sustainable biofuels and high-efficiency, low-emission vehicle engines. The authors would like to thank the U.S. DOE Co-Optima Programs Manager Kevin Stork and Gurpreet Singh for their support and guidance of this work. The YSI work presented in this article was developed based upon funding from the Alliance for Sustainable Energy, LLC, Managing and Operating Contractor for the National Renewable Energy Laboratory for the U.S. Department of Energy.

References

[1] D. Splitter, A. Pawlowski, and R. Wagner, "A historical analysis of the co-evolution of gasoline octane number and spark-ignition engines," *Frontiers in Mechanical Engineering*, vol. 1. Higher Education Press, Jan. 01, 2016. 10.3389/fmech.2015.00016.

[2] J. P. Szybist *et al.*, "What fuel properties enable higher thermal efficiency in spark-ignited engines?," *Progress in Energy and Combustion Science*, vol. 82. Elsevier Ltd, Jan. 01, 2021. 10.1016/j.pecs.2020.100876.

[3] J. E. Parks, J. M. E. Storey, V. Y. Prikhodko, M. M. Debusk, and S. A. Lewis, "Filter-based control of particulate matter from a lean gasoline direct injection engine," in *SAE Technical Papers*, Apr. 2016, vol. 2016-April, no. April. 10.4271/2016-01-0937.

[4] Park C, Lee S, Yi U. Effects of engine operating conditions on particle emissions of lean-burn gasoline direct-injection engine. Energy Nov. 2016;115:1148–55. https://doi.org/10.1016/j.energy.2016.09.051.

[5] Eng JA. Characterization of Pressure Waves in HCCI Combustion. SAE Technical Paper 2002. https://doi.org/10.4271/2002-01-2859.

[6] Dec JE. Advanced compression-ignition engines - Understanding the in-cylinder processes. Proc Combust Inst 2009;vol. 32 II:2727–42. https://doi.org/10.1016/j.proci.2008.08.008.

[7] Kummer JT. Catalysts for automobile emission control. Prog Energy Combust Sci Jan. 1980;6(2):177–99. https://doi.org/10.1016/0360-1285(80)90006-4.

[8] S. Sinha Majumdar and J. A. Pihl, "Impact of Selected High-Performance Fuel Blends on Three-Way Catalyst Light off under Synthetic Spark-Ignition Engine-Exhaust Conditions," *Energy and Fuels*, vol. 34, no. 10, pp. 12900–12910, Oct. 2020, 10.1021/acs.energyfuels.0c02102.

[9] Dagle VL, et al. Production, fuel properties and combustion testing of an iso-olefins blendstock for modern vehicles. Fuel Feb. 2022;310. https://doi.org/10.1016/j.fuel.2021.122314.

[10] Pauly T, Franoschek S, Hoyer R, Eckhoff S. Cost and fuel economy driven aftertreatment solutions -for lean GDI-. SAE Technical Paper 2010. https://doi.org/10.4271/2010-01-0363.

[11] A. B. Dempsey, S. J. Curran, and R. M. Wagner, "A perspective on the range of gasoline compression ignition combustion strategies for high engine efficiency and low NOx and soot emissions: Effects of in-cylinder fuel stratification," *International Journal of Engine Research*, vol. 17, no. 8. SAGE Publications Ltd, pp. 897–917, Oct. 01, 2016. 10.1177/1468087415621805.

[12] Urushihara T, Yamaguchi K, Yoshizawa K, Itoh T. A study of a gasoline-fueled compression ignition engine ~ expansion of HCCI operation range using SI combustion as a trigger of compression ignition. SAE Technical Paper 2005. https://doi.org/10.4271/2005-01-0180.

[13] Manofsky L, Vavra J, Assanis D, Babajimopoulos A. Bridging the gap between HCCI and SI: Spark-assisted compression ignition. SAE Technical Paper 2011. https://doi.org/10.4271/2011-01-1179.

[14] Kalghatgi GT, Ångström H-E. Advantages of fuels with high resistance to auto-ignition in late-injection, low-temperature, compression ignition combustion. SAE Technical Paper 2006. https://doi.org/10.4271/2006-01-3385.

[15] P. Borgqvist, P. Tunestal, and B. Johansson, "Gasoline partially premixed combustion in a light duty engine at low load and idle operating conditions," 2012. 10.4271/2012-01-0687.

[16] Kalghatgi GT, Kumara Gurubaran R, Davenport A, Harrison AJ, Hardalupas Y, Taylor AMKP. Some advantages and challenges of running a Euro IV, V6 diesel engine on a gasoline fuel. Fuel 2013;108:197–207. https://doi.org/10.1016/j.fuel.2012.10.059.

[17] Ketterer JE, Cheng WK. On the nature of particulate emissions from DISI engines at cold-fast-idle. SAE Int J Engines 2014;7(2):986–94. https://doi.org/10.4271/2014-01-1368.

[18] Aikawa K, Sakurai T. Development of a predictive model for gasoline vehicle particulate matter emissions. SAE Int J Fuels Lubr 2010;3:610–22. https://doi.org/10.4271/2010-01-2115.

[19] Aikawa K, Jetter JJ. Impact of gasoline composition on particulate matter emissions from a direct-injection gasoline engine: Applicability of the particulate matter index. Int J Engine Res 2014;15(3):298–306. https://doi.org/10.1177/1468087413481216.

[20] Kim N, Vuilleumier D, He X, Sjöberg M. Ability of Particulate Matter Index to describe sooting tendency of various gasoline formulations in a stratified-charge spark-ignition engine. Proc Combust Inst 2021;38(4):5791–9. https://doi.org/10.1016/j.proci.2020.06.173.

[21] J. Kodavasal, C. P. Kolodziej, S. A. Ciatti, and S. Som, "Computational fluid dynamics simulation of gasoline compression ignition," *Journal of Energy Resources Technology, Transactions of the ASME*, vol. 137, no. 3, 2015, 10.1115/1.4029963.

[22] J. Badra, A. Alhussaini, J. Sim, Y. Viollet, and A. Amer, "Parametric Study to Optimize Gasoline Compression Ignition Operation under Low Load Condition Using CFD," in *SAE Technical Papers*, Apr. 2021, no. 2021. 10.4271/2021-01-0440.

[23] Badra J, Viollet Y, Elwardany A, Im HG, Chang J. Physical and chemical effects of low octane gasoline fuels on compression ignition combustion. Appl Energy Dec. 2016;183:1197–208. https://doi.org/10.1016/j.apenergy.2016.09.060.

[24] Cho K, Zhang Y, Cleary D. Investigation of fuel effects on combustion characteristics of partially premixed compression ignition (PPCI) combustion mode at part-load operations. SAE Int J Engines 2018;11(6):1371–84. https://doi.org/10.2307/26651875.

[25] Badra J, et al. Standardized gasoline compression ignition fuels matrix. SAE Technical Papers 2018;vol:2018-April. https://doi.org/10.4271/2018-01-0925.

[26] Zhang Y, Voice A, Pei Y, Traver M, Cleary D. A computational investigation of fuel chemical and physical properties effects on gasoline compression ignition in a heavy-duty diesel engine. Journal of Solar Energy Engineering, Transactions of the ASME 2018;140(10):Oct. https://doi.org/10.1115/1.4040010.

[27] Badra J, Zubail A, Sim J. Numerical investigation into effects of fuel physical properties on GCI engine performance and emissions. Energy Fuels Oct. 2019;33(10):10267–81. https://doi.org/10.1021/acs.energyfuels.9b02340.

[28] Chuahy FDF, Moses-DeBusk M, Curran SJ, Storey JME, Wagnon SW. The effects of distillation characteristics and aromatic content on low-load gasoline compression ignition (GCI) performance and soot emissions in a multi-cylinder engine. Fuel Sep. 2021;299. https://doi.org/10.1016/j.fuel.2021.120893.

[29] Moses-DeBusk M, Curran SJ, Lewis SA, Connatser RM, Storey JME. Impacts of air-fuel stratification in ACI combustion on particulate matter and gaseous emissions. Emission Control Science and Technology 2019. https://doi.org/10.1007/s40825-019-00122-5.

[30] Heywood JB. Internal combustion engine fundamentals. Second Edition. New York: McGraw-Hill Education; 2018.

[31] Woschni G. A universally applicable equation for the instantaneous heat transfer coefficient in the internal combustion engine. SAE Technical Paper Feb. 1967. https://doi.org/10.4271/670931.

[32] Chang J, et al. New heat transfer correlation for an HCCI engine derived from measurements of instantaneous surface heat flux. SAE Technical Paper Oct. 2004. https://doi.org/10.4271/2004-01-2996.

[33] Yun HJ, Mirsky W. Schlieren-streak measurements of instantaneous exhaust gas velocities from a spark-ignition engine. SAE Technical Paper Feb. 1974;741015. https://doi.org/10.4271/741015.

[34] E. A. Ortiz-Soto, J. Vavra, and A. Babajimopoulos, "Assessment of Residual Mass Estimation Methods for Cylinder Pressure Heat Release Analysis of HCCI Engines with Negative Valve Overlap," Jan. 2011. 10.1115/ICEF2011-60167.

[35] R. P. Fitzgerald, R. Steeper, J. Snyder, R. Hanson, and R. Hessel, "Determination of Cycle Temperatures and Residual Gas Fraction for HCCI Negative Valve Overlap Operation," *SAE International Journal of Engines*, vol. 3, no. 1, Apr. 2010, 10.4271/2010-01-0343.

[36] McEnally CS, et al. Sooting tendencies of co-optima test gasolines and their surrogates. Proc Combust Inst 2019;37(1):961–8. https://doi.org/10.1016/j.proci.2018.05.071.
[37] D. D. Das, P. C. st. John, C. S. McEnally, S. Kim, and L. D. Pfefferle, "Measuring and predicting sooting tendencies of oxygenates, alkanes, alkenes, cycloalkanes, and aromatics on a unified scale," *Combustion and Flame*, vol. 190, pp. 349–364, Apr. 2018, 10.1016/j.combustflame.2017.12.005.
[38] J. Lee, Y. Zhang, T. Tzanetakis, and M. Trever, "Emission Performance of Low Cetane Naphtha as Drop-In Fuel on a Multi-Cylinder Heavy-Duty Diesel Engine and Aftertreatment System," *SAE Technical Paper 2017-01-1000*, 2017, 10.4271/2017-01-1000.
[39] Birch ME, Cary RA. Elemental carbon-based method for monitoring occupational exposures to particulate diesel exhaust. Aerosol Sci Technol Jan. 1996;25(3):221–41. https://doi.org/10.1080/02786829608965393.
[40] May AA, et al. Gas- and particle-phase primary emissions from in-use, on-road gasoline and diesel vehicles. Atmos Environ 2014;88:247–60. https://doi.org/10.1016/j.atmosenv.2014.01.046.
[41] Giechaskiel B, Dilara P, Sandbach E, Andersson J. Particle measurement programme (PMP) light-duty inter-laboratory exercise: Comparison of different particle number measurement systems. Meas Sci Technol 2008;19(9):Sep. https://doi.org/10.1088/0957-0233/19/9/095401.
[42] Saxena S, Chen JY, Dibble R. "Maximizing power output in an automotive scale multi-cylinder homogeneous charge compression ignition (HCCI). engine" 2011. https://doi.org/10.4271/2011-01-0907.
[43] J. Storey *et al.*, "Characterization of Hydrocarbon Emissions from Gasoline Direct-Injection Compression Ignition Engine Operating on a Higher Reactivity Gasoline Fuel," *SAE International Journal of Engines*, vol. 10, no. 4, Mar. 2017, 10.4271/2017-01-0747.
[44] Hill PG, Mctaggart-Cowan GP. Nitrogen oxide production in a diesel engine fueled by natural gas. SAE Technical Paper 2005–01-1727, 2005,. https://doi.org/10.4271/2005-01-1727.
[45] F. Leach, V. Shankar, M. Davy, and M. Peckham, "The Influence of Cycle-to-Cycle Hydrocarbon Emissions on Cyclic NO:NO2 Ratio from a HSDI Diesel Engine," Nov. 2020. 10.1115/ICEF2020-2904.
[46] M. Hori, N. Matsunaga, N. Marinov, P. William, and W. Charles, "An experimental and kinetic calculation of the promotion effect of hydrocarbons on the NO-NO2 conversion in a flow reactor," *Symposium (International) on Combustion*, vol. 27, no. 1, Jan. 1998, 10.1016/S0082-0784(98)80427-X.
[47] M. Hori, Y. Koshiishi, N. Matsunaga, P. Glaude, and N. Marinov, "Temperature dependence of NO to NO2 conversion by n-butane and n-pentane oxidation," *Proceedings of the Combustion Institute*, vol. 29, no. 2, Jan. 2002, 10.1016/S1540-7489(02)80270-X.
[48] A. Frassoldati, T. Faravelli, and E. Ranzi, "Kinetic modeling of the interactions between NO and hydrocarbons at high temperature," *Combustion and Flame*, vol. 135, no. 1–2, Oct. 2003, 10.1016/S0010-2180(03)00152-4.
[49] X. Yu, S. Yu, and M. Zheng, "Hydrocarbon impact on NO to NO $_2$ conversion in a compression ignition engine under low-temperature combustion," *International Journal of Engine Research*, vol. 20, no. 2, Feb. 2019, 10.1177/1468087417745441.
[50] Bergman M, Fredriksson J, Golovitchev VI. CFD-based optimization of a diesel-fueled free piston engine prototype for conventional and HCCI combustion. SAE Int J Engines 2008;1(1):Oct. https://doi.org/10.4271/2008-01-2423.
[51] Benajes J, López JJ, Novella R, Redón P. Comprehensive modeling study analyzing the insights of the NO-NO 2 conversion process in current diesel engines. Energy Convers Manage 2014;84:691–700. https://doi.org/10.1016/j.enconman.2014.04.073.
[52] N. Gupta, X. Yu, N. Eaves, M. Wang, and M. Zheng, "Numerical Investigation on NO to NO $_2$ Conversion in a Low-Temperature Combustion CI Engine," *SAE Technical Paper 2021-01-0506*, Apr. 2021, 10.4271/2021-01-0506.
[53] Daham B, et al. Application of a portable FTIR for measuring on-road emissions. SAE Technical Paper 2005–01-0676, Apr 2005. https://doi.org/10.4271/2005-01-0676.
[54] T. Wallner and R. Frazee, "Study of Regulated and Non-Regulated Emissions from Combustion of Gasoline, Alcohol Fuels and their Blends in a DI-SI Engine," *SAE Technical Paper 2010-01-1571*, May 2010, 10.4271/2010-01-1571.
[55] T. Wallner, "Correlation between speciated hydrocarbon emissions and flame ionization detector response for gasoline/alcohol blends," *Journal of Engineering for Gas Turbines and Power*, vol. 133, no. 8, 2011, 10.1115/1.4002893.
[56] N. Wright, D. Osborne, and N. Music, "Comparison of Hydrocarbon Measurement with FTIR and FID in a Dual Fuel Locomotive Engine," *SAE Technical Paper 2016-01-0978*, Apr. 2016, 10.4271/2016-01-0978.
[57] S. Lewis, J. Storey, R. Connatser, S. Curran, and M. Moses-DeBusk, "Detection of Polar Compounds Condensed on Particulate Matter Using Capillary Electrophoresis-Mass Spectrometry," *SAE Technical Paper 2020-01-0395*, Apr. 2020, 10.4271/2020-01-0395.
[58] Burke S, Rhoads R, Ratcliff M, McCormick R, Windom B. Measured and predicted vapor liquid equilibrium of ethanol-gasoline fuels with insight on the influence of azeotrope interactions on aromatic species enrichment and particulate matter formation in spark ignition engines. SAE Technical Papers 2018;vol:2018-April. https://doi.org/10.4271/2018-01-0361.
[59] Ratcliff MA, et al. Impact of ethanol blending into gasoline on aromatic compound evaporation and particle emissions from a gasoline direct injection engine. Appl Energy Sep. 2019;250:1618–31. https://doi.org/10.1016/j.apenergy.2019.05.030.
[60] T. R. Powell *et al.*, "Octane index applicability over the pressure-temperature domain," *Energies (Basel)*, vol. 14, no. 3, Feb. 2021, 10.3390/en14030607.
[61] Storey JM, Barone T, Norman K, Lewis S. Ethanol blend effects on direct injection spark- ignition gasoline vehicle particulate matter emissions. SAE Int J Fuels Lubr 2010;3(2):650–9. https://doi.org/10.4271/2010-01-2129.
[62] Maricq MM, Szente JJ, Jahr K. The impact of ethanol fuel blends on PM emissions from a light-duty GDI vehicle. Aerosol Sci Technol 2012;46(5):576–83. https://doi.org/10.1080/02786826.2011.648780.
[63] West B, Huff S, Moore L, Debusk M, Sluder S. "Effects of high-octane E25 on two vehicles equipped with turbocharged. Direct-Injection Engines" 2018. https://doi.org/10.2172/1470897.
[64] Maricq MM, Xu N. The effective density and fractal dimension of soot particles from premixed flames and motor vehicle exhaust. J Aerosol Sci 2004;35(10):1251–74. https://doi.org/10.1016/j.jaerosci.2004.05.002.
[65] Xue J, et al. Using a new inversion matrix for a fast-sizing spectrometer and a photo-acoustic instrument to determine suspended particulate mass over a transient cycle for light-duty vehicles. Aerosol Sci Technol 2016;50(11):1227–38. https://doi.org/10.1080/02786826.2016.1239247.